Blowout bifurcations and the onset of magnetic dynamo action*

David Sweet, Edward Ott,[†,a)] Thomas M. Antonsen, Jr.,[a)] and Daniel P. Lathrop
Institute for Plasma Research and Department of Physics, University of Maryland, College Park, Maryland 20742

John M. Finn
Los Alamos National Laboratory, Los Alamos, New Mexico 87544

This paper numerically investigates the magnetohydrodynamic equations in three dimensions with periodic boundary conditions in a parameter range where a forced fluid flow is chaotic. It is found that the transition to *dynamo action*, whereby the magnetic field is sustained by interaction with the forced flow, is a *blowout bifurcation*. The blowout bifurcation is typified by bursting behavior, or ''on-off intermittency.'' In particular, near the transition there are short, intermittently occurring bursts of strong magnetic field activity where the total magnetic energy is comparable to the total flow kinetic energy. Between these bursts the magnetic energy is very small. As one approaches the transition from the dynamo-active side, the time between bursts becomes longer and longer, approaching infinity at the transition. Numerical verification is given for the presence of signature scaling laws in numerical computations utilizing a pseudospectral model with triply periodic boundary conditions. This work implies specific testable predictions for experimental dynamos. © *2001 American Institute of Physics.* [DOI: 10.1063/1.1342228]

I. INTRODUCTION

It is believed that the magnetic fields of the Earth and Sun are created by *dynamo action*, whereby the kinetic energy of a convection-driven flow of an electrically conducting fluid is converted into magnetic energy.[1] This system, called a *magnetohydrodynamic (MHD) dynamo*, has been the subject of intense study.[2–8]

A number of groups are pursuing experimental programs aimed at the realization of dynamo action in the laboratory.[9–14] The efforts in Riga[9] and Karlsruhe[10] self-generate in constrained geometries which severely limit the turbulent fluctuations by internal walls. Other efforts, in Cadarache,[11] Madison,[12] Socorro,[13] and College Park,[14] have (or are planned to have) relatively unconstrained stirred flows in liquid sodium with typical hydrodynamic Reynolds numbers of $R \sim 10^7$ leading to a vigorous turbulent flow. The transition to dynamo action in these unconstrained systems will be strongly influenced by the turbulent character of the flow.

It is to be expected that as the forcing and/or size of such experiments is increased or the geometry is made more favorable, a transition to dynamo action will be achieved. The object of this article is to investigate what the character of this transition will be. We find that a likely scenario is that the transition to dynamo action will be via a type of bifurcation called a *blowout bifurcation*, one which has been studied in other settings.[15–24] Based on this, it is to be expected that the transition will be characterized by intermittently bursting magnetic fields which obey scaling laws (explained subsequently) near the transition. In particular, near the transition

there are short, intermittently occurring bursts of strong magnetic field activity where the total magnetic energy is comparable to the total flow kinetic energy. Between these bursts the magnetic energy is very small. As one approaches the transition from the dynamo-active side, the time between bursts becomes longer and longer, approaching infinity at the transition. This is illustrated by the results in Figs. 1(a) and 1(b) from our three-dimensional numerical dynamo computation (described in Sec. III), which shows $b(t)$ (a global measure of the magnetic field strength, see Sec. IV) versus time for two parameter values just past the onset of dynamo action. The parameter value of Fig. 1(b) is closer by a factor of 2.5 to the critical onset value than is the parameter value of Fig. 1(a). Correspondingly, we observe that bursting is less frequent in Fig. 1(b) than in Fig. 1(a). The previous discussions of blowout bifurcations have occurred in the context of chaotic dynamical systems. For the purposes of our discussion, and to make contact with the language used in previous discussions of blowout bifurcations, we shall refer to a turbulent fluid flow as chaotic. (While chaos is often thought of as resulting from low-dimensional systems, and turbulence is often thought of as being ''high dimensional'' or as possessing ''many active degrees of freedom,'' this distinction is not necessary in the present context.)

In our studies we use the following nondimensional MHD equations:

$$\frac{\partial \mathbf{v}}{\partial t} + (\mathbf{v} \cdot \nabla)\mathbf{v} = -\nabla p + R^{-1}\nabla^2 \mathbf{v} + (\nabla \times \mathbf{B}) \times \mathbf{B} + \mathbf{F}(\mathbf{x}),$$
(1)

$$\frac{\partial \mathbf{B}}{\partial t} + (\mathbf{v} \cdot \nabla)\mathbf{B} = (\mathbf{B} \cdot \nabla)\mathbf{v} + R_m^{-1}\nabla^2 \mathbf{B}.$$
(2)

Equation (1) is the Navier–Stokes equation with additional terms representing the Lorentz force and an external force,

FIG. 2. $b(t)$ vs t. When the magnetic Reynolds number, $R_m = 7.81$, is slightly below the transition value and a small external magnetic field is applied, $B_0 = 1.6 \times 10^{-3}$, $b(t)$ displays intermittent bursting. [When no external field is applied, $b(t)$ does not show sustained burst activity, but, rather, eventually decays to zero.]
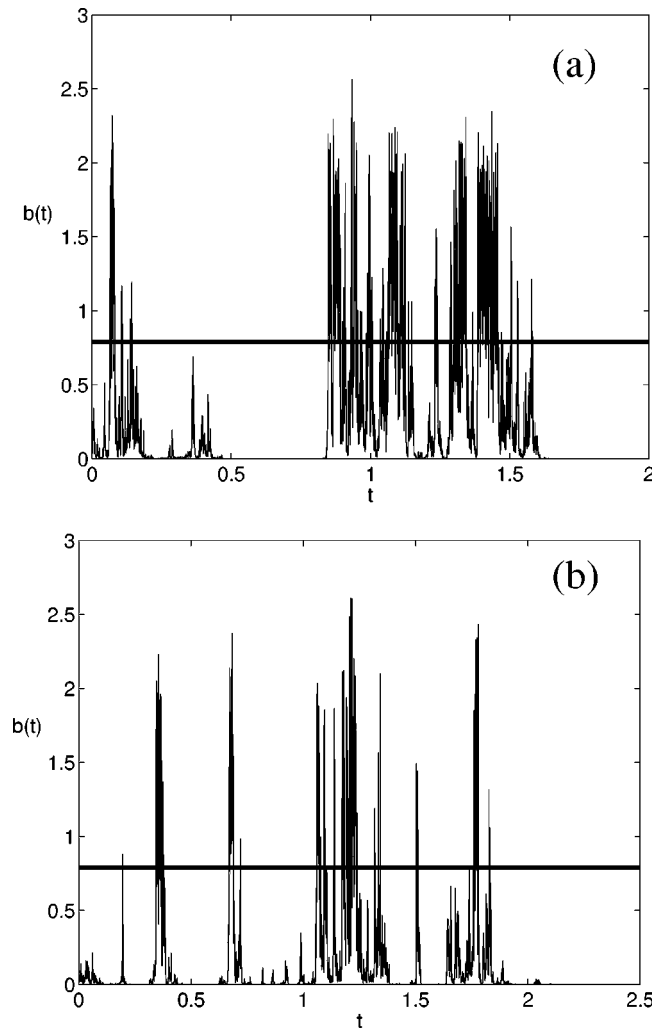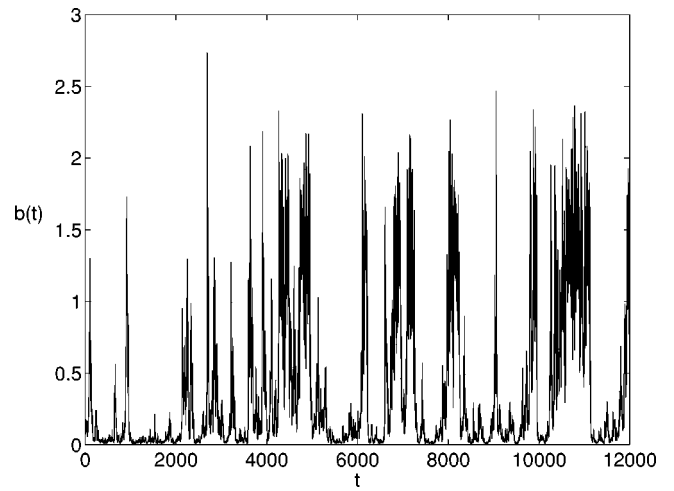
FIG. 1. (a) $b(t)$ vs t, where t is in units of 10^4 time steps. The trace of $b(t)$ bursts when the magnetic Reynolds number, $R_m = 8.06$, is slightly above the transition value. A burst is defined as the time when $b(t)$ crosses a threshold value (shown here at $b_0 = 0.8$ by a horizontal line). (b) A similar figure with $R_m = 7.96$, closer to the transition value of $R_{mc} \approx 7.88$ (but still above transition). Note that the maximum value of b is about 2.5 while $\bar{v}$ is of the same order (from Fig. 6, typically about 5), implying that the magnetic energy at nonlinear saturation is of the order of the flow kinetic energy.

and Eq. (2) is the magnetic induction equation, derived from Faraday's law, Ampere's law, and Ohm's law, and the assumption that the fluid is incompressible:

$$\nabla \cdot \mathbf{v} = 0. \tag{3}$$

The parameters R and R_m are the hydrodynamic and magnetic Reynolds numbers. The external force $\mathbf{F}(\mathbf{x})$ in (1) is described in Sec. III.

II. BACKGROUND

The bifurcation we are discussing is the transition from a nondynamo system (i.e., the total magnetic energy always decays to zero) with chaotic time variation of the flow field to a dynamo system with chaotic time variation of the flow and the magnetic energy.

The most striking feature of this type of bifurcation is bursting (so-called on–off intermittency).[15,17–23] In our sys-

tem we observe bursting of the magnetic energy when (a) the magnetic Reynolds number is just above the transition value (Fig. 1) or (b) the magnetic Reynolds number is just below the transition value and a small external magnetic field is applied to the system (Fig. 2).

We now give some background on blowout bifurcations. We consider a dynamical set of equations evolving the system state forward in time. We imagine a given state of the system to be a point in the phase space of the system. For example, in the dynamo context, the dynamical system is Eqs. (1)–(3) plus boundary conditions, and the system state at time t is given by the vector fields $\mathbf{v}(\mathbf{x},t)$ and $\mathbf{B}(\mathbf{x},t)$ (i.e., by the magnitudes and directions of $\mathbf{v}$ and $\mathbf{B}$ at each point in space). Thus, the phase space is, in principle, infinite dimensional (a function space).

Attributes which characterize a system possessing a blowout bifurcation are as follows. (i) There is an invariant manifold in the phase space of the system. [By an invariant manifold we mean a subset of the phase space where the subset is a smooth hypersurface such that if an initial condition (state) is placed on the hypersurface, then the subsequently evolving state remains on the hypersurface for all time.] (ii) Initial conditions placed on the invariant hypersurface evolve to chaotic solutions (i.e., there is a chaotic attractor for such initial conditions). (iii) For parameter values below the critical value at which the blowout bifurcation occurs (in the context of the dynamo, $R_m < R_{mc}$, where R_{mc} is the critical magnetic Reynolds number), the chaotic motion in the invariant manifold is attracting in the full phase space in the sense that almost all infinitesimal perturbations of the chaotic motion in the directions transverse to the invariant manifold decay exponentially in a suitable average sense. Here, by this we mean that the Lyapunov exponents for perturbations from the chaotic attractor in the invariant surface are negative when those perturbations are transverse to the invariant surface. (iv) As a parameter value increases through the critical blowout value (e.g., R_m increases through

R_{mc}) one of the transverse Lyapunov exponents increases from negative values (for $R_m < R_{mc}$) to positive values (for $R_m > R_{mc}$). Thus, the chaotic attractor for initial conditions in the invariant manifold loses its average stability to transverse perturbations. [While we refer to chaos on the invariant manifold, we should note that the role of chaos in the blowout bifurcation can be replaced by suitable (nondeterministic) stochastic processes with no essential change in the blowout bifurcation phenomena (see Sec. IV A and Refs. 15 and 20).]

The presence of an invariant mainfold allows one to define local transverse variables (i.e., variables measuring the distances locally orthogonal to the manifold) and approximate their dynamics near the manifold as linear. The on-manifold motion generically influences the transverse variables by altering their growth rates. That is, small transverse displacements from a state on the invariant manifold generically increase or decrease at different local, linear growth rates depending on where the state is located on the invariant manifold. Since the motion on the invariant manifold is chaotic, these local, linear growth rates are changed in an effectively random manner. This situation for small deviations from the invariant manifold, coupled with nonlinearity for large transverse deviations, implies various signature scaling laws (discussed in Sec. IV)[15,17,19–22] which are characteristic of blowout bifurcations.

We now discuss how the problem of MHD dynamo onset corresponds to conditions (i) and (ii) for a blowout bifurcation. Setting $\mathbf{B}=0$ we obtain the usual Navier–Stokes equations (the Lorentz force term is zero for $\mathbf{B}=0$). In particular, $\mathbf{B}=0$ is a solution of (2), and this represents an invariant manifold in the full $\mathbf{B}-\mathbf{v}$ phase space. Thus, condition (i) for a blowout bifurcation is satisfied. For sufficiently large fluid Reynolds number, R, the (magnetic field-free) Navier–Stokes equations are typically turbulent. That is, the system evolution is chaotic on the invariant manifold $\mathbf{B}=0$ [condition (ii)].

With respect to conditions (iii) and (iv), refer to Fig. 3, which shows the results of numerical computations of the largest transverse Lyapunov exponent h versus R_m, with R and $\mathbf{F}(\mathbf{x})$ chosen so that $\mathbf{v}$ behaves chaotically in time (see Sec. III for details). The transverse Lyapunov exponent is denoted h and is computed by setting $\mathbf{B}=0$ in (1) (the Lorentz force is quadratic in $\mathbf{B}$ and hence is absent to linear order) and solving the resulting set of equations (1)–(3) for the linear evaluation of the magnetic field perturbation $\delta\mathbf{b}$. (This problem is commonly referred to as the kinematic dynamo problem.[2–4,6–8]) We see from Fig. 3 that as R_m is increased there is a transition from negative h to positive h. The value of R_m at which this transition occurs is the critical value for dynamo onset R_{mc}. Below R_{mc}, initial magnetic field perturbations all eventually decay to zero [condition (iii)]. Note, however, that for $R_m < R_{mc}$, although there is always eventual decay to $\mathbf{B}=0$ (i.e., to the invariant manifold), the magnetic field time evolution may show finite stretches of time where growth takes place. For $R_m > R_{mc}$, infinitesimal perturbations from $\mathbf{B}=0$ tend to grow on average [condition (iv)], and our fully nonlinear numerical com-
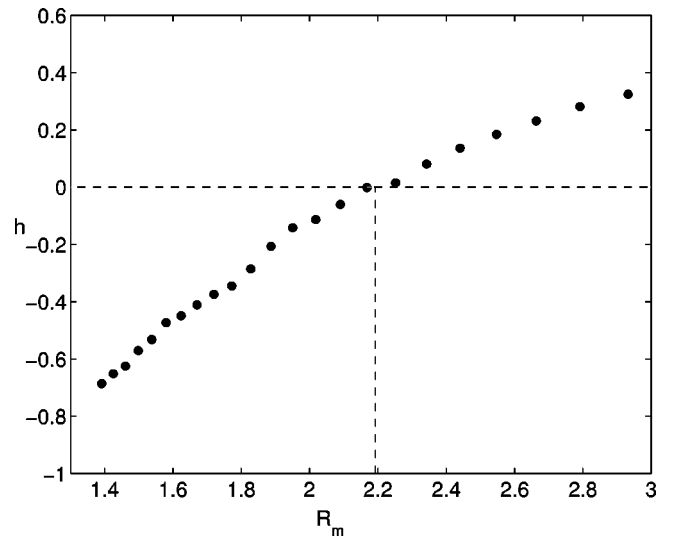

FIG. 3. Transverse Lyapunov exponent (h) as a function of magnetic Reynolds number, R_m. The data points were calculated from 572 kinematic LOM simulations [i.e., linearized simulations in which the Lorentz force on the right-hand side of Eq. (1) is omitted] started from independent, random initial conditions, using various values of R_m. The estimate of h for a given value of R_m is taken to be the average of the straight-line fits to the plots of $\log b(t)$ vs t for all simulations (typically four) taken at a given value of R_m. [The length of the simulations varied depending on the growth rate experienced by the magnetic field during that simulation. The magnetic field was allowed to grow to $b(t)/b(0) \cong 10^{300}$ for $R_m > R_{mc}$ or decay to $b(t)/b(0) \cong 10^{-300}$, for $R_m < R_{mc}$ where these limits are those of IEEE double-precision numbers.] The transition to dynamo action occurs as R_m passes from $R_m < R_{mc} \cong 2.193$ to $R_m > R_{mc}$.

putations of solutions of Eqs. (1)–(3) indicate strongly fluctuating large magnetic fields persisting for all time (Fig. 1).

We emphasize the difference between the finite time magnetic field instability growth rate (or Lyapunov exponent) and its infinite time limit. Specifically, for a particular $t=0$ infinitesimal perturbation, $\delta\mathbf{b}(\mathbf{x},0)$, the finite time Lyapunov exponent for the time interval t to $t+\tau$ is

$$h_\tau(\delta\mathbf{b}(\mathbf{x},0),t) = \frac{1}{\tau}\ln[\|\delta\mathbf{b}(\mathbf{x},t+\tau)\|/\|\delta\mathbf{b}(\mathbf{x},t)\|] \qquad (4)$$

and the infinite time exponent is

$$h = \lim_{\tau\to\infty} h_\tau(\delta\mathbf{b}(\mathbf{x},0),t). \qquad (5)$$

Note that the infinite time exponent is presumed to be the same for all choices of t and almost all choices of the initial perturbation $\delta\mathbf{b}(\mathbf{x},0)$. Thus, the infinite time exponent has a definite numerical value. The finite time exponent, in contrast, fluctuates with t. One experimental group[14] has measured the probability distribution for these fluctuating finite time exponents h_τ. They do this by applying a magnetic pulse of fixed strength and fitting a straight line to a semilog plot of the measured, decaying magnetic field strength versus time over a time interval of length τ. h_τ is the slope of this line. (Because their experimental R_m is relatively far below R_{mc}, the h_τ values they determine are all negative.) Repeating this many times they obtain many values of h_τ from which they construct, via the histogram method, their experimental probability distribution function. This distribution is
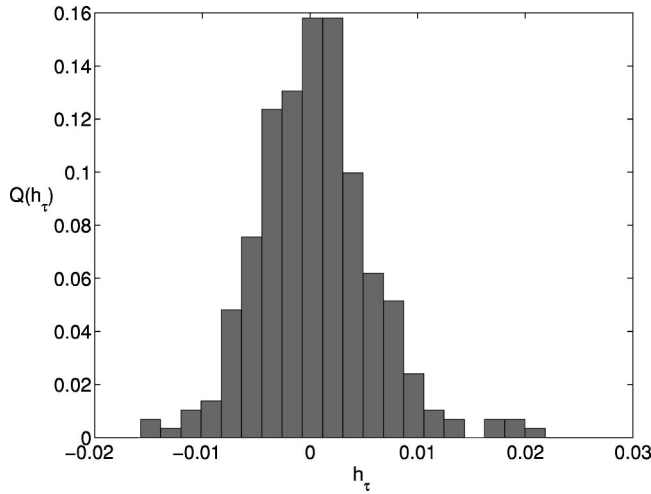
FIG. 4. Probability distribution function, $Q(h_\tau)$, of finite-time transverse Lyapunov exponents, h_τ, for $\tau=5$ (giving 578 samples) and $R_m=7.96$, slightly above transition, $R_{mc}=7.88$. The average value of h_τ in this distribution is $\langle h_\tau \rangle = 2.80 \times 10^{-3}$. We estimate that $D=0.02$.
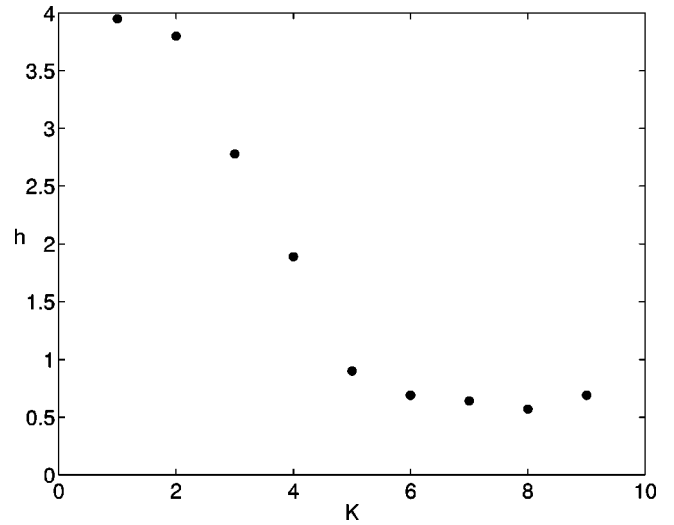

FIG. 5. Magnetic field growth rate, h, vs largest mode in simulation, K. The simulation appears to have converged at $K=6$. All simulations for this figure were performed with $R_m=12.6$.

well fit by a Gaussian. This very graphically illustrates the expected stochastic nature of the growth/decay of small magnetic field perturbations, and is one of the key aspects of the dynamics necessary for a blowout bifurcation. We also see such a distribution in our simulation (see Fig. 4). In our simulation (as in the experiment of Ref. 14) it is the chaotic flow field (i.e., motion on the invariant manifold) that gives rise to the distribution.

III. COMPUTER SIMULATION

We use a pseudospectral method to simulate Eqs. (1)–(3), as described in Refs. 25–27, which consists of a set of first-order ordinary differential equations (ODEs) governing the evolution of the coefficients of spatial Fourier expansions of $\mathbf{v}(\mathbf{x},t)$ and $\mathbf{B}(\mathbf{x},t)$. We expand the solution to Eqs. (1)–(3) [i.e., the pair of vectors $\mathbf{v}(\mathbf{x},t)$ and $\mathbf{B}(\mathbf{x},t)$] in truncated Fourier series

$$\mathbf{v}(\mathbf{x},t)=\sum_{k_x=-K}^{K}\sum_{k_y=-K}^{K}\sum_{k_z=-K}^{K}\mathbf{v_k}(t)e^{i\mathbf{k}\cdot\mathbf{x}},$$

$$\mathbf{B}(\mathbf{x},t)=\sum_{k_x=-K}^{K}\sum_{k_y=-K}^{K}\sum_{k_z=-K}^{K}\mathbf{B_k}(t)e^{i\mathbf{k}\cdot\mathbf{x}},$$

with truncation at mode number K in each component of $\mathbf{k}$ (where k_x, k_y, k_z are integers). The sets of solutions accessible to this method, therefore, are those for which $\mathbf{v}$ and $\mathbf{B}$ are spatially periodic with period 2π and have structures no smaller than $2\pi/K$.

The partial differential equations (PDEs) given by Eqs. (1)–(3) then become the set of ODEs:

$$\frac{\partial \mathbf{v_k}}{\partial t}=-\nu|\mathbf{k}|^2\mathbf{v_k}+\mathbf{f_k}+\mathbf{g_k}+\mathbf{F_k}-\mathbf{k}\frac{\mathbf{k}\cdot(\mathbf{f_k}+\mathbf{g_k}+\mathbf{F_k})}{|\mathbf{k}|^2},$$

$$\frac{\partial \mathbf{B_k}}{\partial t}=-\lambda|\mathbf{k}|^2\mathbf{B_k}+\mathbf{r_k}-\mathbf{s_k},$$

$$(6)$$

where

$$f_{\mathbf{k},\alpha}=-i\sum_{\beta} k_\beta \sum_{\mathbf{m}+\mathbf{n}=\mathbf{k}} v_{\mathbf{m},\beta}v_{\mathbf{n},\alpha}, \tag{7}$$

$$g_{\mathbf{k},\alpha}=i\sum_{\beta} k_\beta \sum_{\mathbf{m}+\mathbf{n}=\mathbf{k}} B_{\mathbf{m},\beta}B_{\mathbf{n},\alpha}, \tag{8}$$

$$r_{\mathbf{k},\alpha}=i\sum_{\beta} k_\beta \sum_{\mathbf{m}+\mathbf{n}=\mathbf{k}} v_{\mathbf{m},\beta}B_{\mathbf{n},\alpha}, \tag{9}$$

$$s_{\mathbf{k},\alpha}=i\sum_{\beta} k_\beta \sum_{\mathbf{m}+\mathbf{n}=\mathbf{k}} B_{\mathbf{m},\beta}v_{\mathbf{n},\alpha}, \tag{10}$$

where the final term in Eq. (6) is the form of $-\nabla p$ that is required when one insists that condition (3) hold. The simulation consists of evolving this set of Fourier coefficients forward in time with a fourth-order, adaptive time-step, Runge–Kutta integrator.

The nonlinear terms, Eqs. (7)–(10) are convolutions and are evaluated when needed by transforming the variables to real space using a fast Fourier transform (FFT), performing a pointwise product, and transforming back to Fourier space using an inverse FFT.

The parameter values used were $R=6.32$, $K=6$, and R_m was varied from 7.81 to 8.16. There are $(2K+1)^3-1$ excited $\mathbf{k}$ vectors which, for $K=6$, yields 2196 excited $\mathbf{k}$ vectors. For the value $K=6$, the simulation is converged in K. We tested for convergence by measuring the growth rate of the magnetic energy for a case with $R_m=12.6$, somewhat above R_{mc}, using the kinematic dynamo simulation (starting from random initial conditions) at successive, increasing values of K. The results are shown in Fig. 5.

Due to the large amount of computation needed to verify one of the scaling laws, a lower-order model (LOM), with $K=1$, was employed for the purpose of comparison with that scaling prediction. For all other purposes a higher-order model with $K=6$ (HOM) was used. [While the LOM is not converged, it shows the same qualitative and scaling behaviors as found in the higher-order model (HOM).]
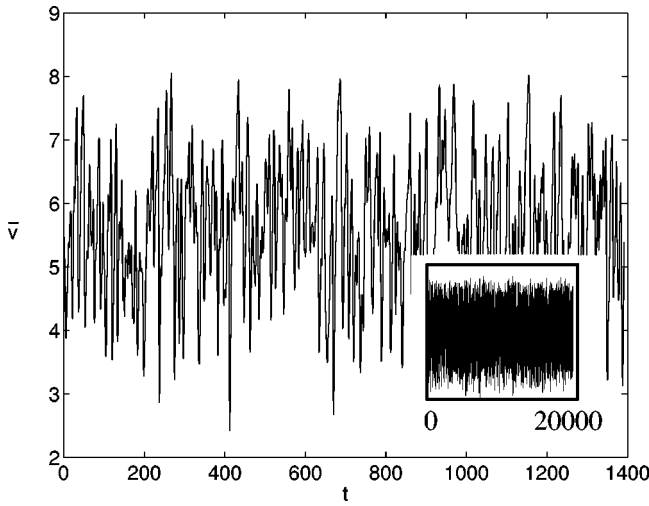
FIG. 6. Norm of the flow velocity versus time where $\bar{v} \equiv \sqrt{\Sigma_\mathbf{k} |\mathbf{v_k}|^2}$. The inset shows a much longer trace, $0 < t < 2 \times 10^4$, showing that this behavior persists for long times. We measured the largest Lyapunov exponent for this trace to be $h_v = 0.41$, which, since $h_v > 0$, shows that the motion is chaotic. This trace was taken from a fluid-only simulation with Reynolds number $R = 6.3$.

The forcing term, $\mathbf{F_k}$, has the form

$$\mathbf{F}_{(0,0,\pm 1)} = \tfrac{1}{2}(\hat{y} \mp i\hat{x}),$$

$$\mathbf{F}_{(\pm 1,0,0)} = \tfrac{1}{2}(\hat{z} \mp i\hat{y}),$$

$$\mathbf{F}_{(0,\pm 1,0)} = \tfrac{1}{2}(\hat{x} \mp i\hat{z}).$$

For $\mathbf{B} = 0$, if the flow is assumed to be time independent, this forcing yields the so-called ABC flow[4,5,28] given by $\mathbf{v_k} = R\mathbf{F_k}/|\mathbf{k}|^2$. For $R = 6.32$, the ABC flow is unstable. Non-forced flow modes are coupled to the forced modes by the nonlinear term, $\mathbf{f_k}$, Eq. (7), and the resulting flow exhibits Eulerian chaos. That is, the Fourier coefficients $\mathbf{v_k}(t)$ and $\mathbf{B_k}(t)$ evolve chaotically in time. Figure 6 shows a trace of $\bar{v} \equiv \sqrt{\Sigma |\mathbf{v_k}|^2}$ versus time for, $R_m = 7.88$, a non-dynamo-action parameter value. This flow was verified to be chaotic by computing the largest Lyapunov exponent to be $h_v = 2.92 > 0$. We define h_v by

$$|\delta\mathbf{v_k}| \sim e^{h_v t}$$

for infinitesimal separations between initial conditions, $\delta\mathbf{v_k}$. We compute $\delta\mathbf{v_k}$ by linearizing Eq. (1) with $\mathbf{B} = 0$ and integrating until $|\delta\mathbf{v_k}|$ has grown by a factor of $\sim 10^{300}$. We estimate h_v by the slope of a straight line fit to a log-linear plot of $|\delta\mathbf{v_k}|$ vs t.

IV. PREDICTION AND RESULTS

A. Model for intermittent bursting

A convenient way to analyze blowout bifurcations is through a simple model which we will describe in what follows.[15,21,22] The motivation for using the simple model is that it is suspected that it yields the same phenomenology and scalings as real situations. In the language of statistical physics, typical situations yielding blowout bifurcations are in the same universality class as this model. Our numerical results and past work[15,19,21,22] support this hypothesis. The

model uses a discrete time variable, $t = 0,1,2,...$, and advances a non-negative variable $\hat{b}_t$ [analogous to $b(t)$ in Fig. 1] forward in time by a linear stochastic rule

$$\hat{b}_{t+1} = \eta_t \hat{b}_t \tag{11}$$

if $\hat{b}_{t+1} \leq 1$. Here $\eta_t \geq 0$ is a growth factor randomly chosen at each time t according to some probability distribution function. If (11) ever gives $\hat{b}_{t+1} > 1$, then $\hat{b}_{t+1}$ is set equal to one. This nonlinear aspect of the model reflects, for example, the physical saturation mechanism in the dynamo whereby the maximum value attainable by the magnetic field energy, $E_B(t)$, is limited to be of the order of the total fluid flow kinetic energy. Introducing $z_t = \log(1/\hat{b}_t)$ and $\xi_t = \log(\eta_t)$, Eq. (11) yields a random walk in $z \geq 0$,

$$z_{t+1} = z_t - \xi_t, \tag{12}$$

with an impenetrable boundary at $z = 0$ (from the upper bound on $\hat{b}$, $\hat{b} \leq 1$). For a given realization of the random process ξ_t, finite time (τ) Lyapunov exponents for (11) are given by

$$\hat{h}_\tau = \frac{1}{\tau} \sum_{t=T}^{T+\tau} \xi_t.$$

Evaluating $\hat{h}_\tau$ for many values of T, we can obtain a distribution function for $\hat{h}_\tau$ [analogous to the distribution $Q(h_\tau)$ in Fig. 4]. In the limit that $\tau \to \infty$, this distribution function approaches a delta function at the usual (infinite time) Lyapunov exponent. That is, with probability one, a given realization of the random process ξ_t yields

$$\hat{h} = \lim_{\tau \to \infty} \hat{h}_\tau$$

independent of the starting time T [see also Eq. (5)]. For finite τ, however, there is a spread of $\hat{h}_\tau$ values about $\hat{h}$ which decreases to zero as τ becomes large:

$$\langle (\hat{h}_\tau - \hat{h})^2 \rangle \sim 2D/\tau. \tag{13}$$

In Eq. (13) the quantity D is the diffusion coefficient associated with the random walk (12), $D = \langle \xi^2 \rangle/2$. We note that by fitting a straight line to $\tau^2 \langle (h_\tau - h)^2 \rangle$ vs τ for our dynamo we can use Eq. (13) to obtain a numerical estimate of the diffusion coefficient[29] D for our problem (or any blowout bifurcation problem). In particular, we use Eq. (4) and Eqs. (6)–(10) linearized about $\mathbf{B} = 0$ to compute h_τ at fixed τ and many different times t. The variance of this collection of h_τ values yields an estimate of $\langle (h_\tau - \langle h_\tau \rangle)^2 \rangle$ and, via histogramming, we can also estimate the probability distribution function $Q(h_\tau)$ in Fig. 4.

Analysis of the simple model above yields results which we summarize in the next subsection.

B. Predicted scalings just above transition ($R_m > R_{mc}$)

In Refs. 15, 17, and 19–22 various scaling relations are predicted for blowout bifurcations, all of which can be derived using the simple stochastic model of Sec. IV A. We

summarize the blowout scaling results relevant to our studies for $R_m > R_{mc}$, where in all cases it is presumed that $(R_m - R_{mc})/R_m \ll 1$.

(1) *Time average distance from the invariant manifold.* We define a magnetic field norm, $b(t) \equiv [\Sigma_{\mathbf{k}} |\mathbf{B_k}|^2]^{1/2} = [\Omega^{-1} \iiint_\Omega |\mathbf{B}(x,y,z,t)|^2 dxdydz]^{1/2}$, where $\Omega = (2\pi)^3$ is the simulation volume. Thus, $b(t)$ provides an instantaneous global measure of the magnetic field activity over the simulation volume. The quantity $b(t)$ is related to the total magnetic energy, $E_B(t)$, by $E_B(t) = 1/2\Omega b(t)^2$. Alternatively, $b(t)$ is the Euclidean distance of the system state from the $\mathbf{B} = 0$ invariant manifold. Let $\langle b(t) \rangle$ denote the time average of the bursting time series $b(t)$ vs t (see Fig. 1). Then $\langle b(t) \rangle$ is predicted[15] to scale linearly with $(R_m - R_{mc})$,

$$\langle b(t) \rangle \sim (R_m - R_{mc})/R_{mc}. \tag{14}$$

As $(R_m - R_{mc})$ increases from zero, $\langle b(t) \rangle$ increases due to the greater frequency of bursts, while b_{max}, the maximum value of $b(t)$ observed over a long time series consisting of many bursts, remains essentially constant.

(2) *Fractality of the set of burst times.* We define the burst times as the set of times at which $b(t)$ crosses some threshold value b_0 in the upward direction; see Fig. 1(a) where the chosen threshold value is shown as a horizontal line, $b = b_0$. In general, we can choose the threshold to be some $O(1)$ fraction β of b_{max} (i.e., $b_0 = \beta B_{max}$) and the scalings based on this thresholding [Eqs. (15)–(19)] are independent of the choice of $\beta < 1$.

Imagine that we plot the burst times along the t axis between $t = 0$ and some very long time $t = T$, and then we rescale this long time interval to the unit interval by normalizing t to T. In that case, in the double limit $T \rightarrow \infty$ followed by $(R_m - R_{mc}) \rightarrow 0^+$, the set of normalized burst times in the unit interval is predicted[22] to approach a fractal set with box-counting dimension

$$d = \tfrac{1}{2}. \tag{15}$$

Without normalizing time and considering $(R_m - R_{mc})$ to be small but nonzero, this corresponds to

$$N(\delta t) \sim (\delta t)^{-d}, \tag{16}$$

where the t axis has been divided into segments of length δt, and $N(\delta t)$ is the number of these segments that is needed to cover the set of burst times. This scaling is valid in the range

$$D^{-1} \ll \delta t \ll \frac{D}{h^2}, \tag{17}$$

where h is the average transverse Lyapunov exponent Eq. (5).

(3) *Distribution of interburst intervals.* Let t_j and t_{j+1} be two successive burst times as described above. The jth interburst interval is defined as $\Delta_j = t_{j+1} - t_j$, and, given many burst times, we can use the histogram procedure to obtain a probability distribution function for the interburst intervals, $P(\Delta)$. This probability distribution is predicted to have a $-\tfrac{3}{2}$ power law form,
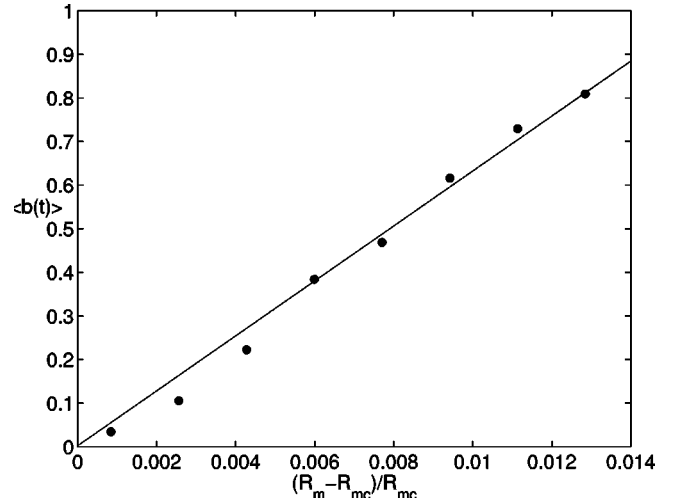
$$P(\Delta) \sim \Delta^{-3/2}, \tag{18}$$

in the range

FIG. 7. $\langle b(t) \rangle \sim (R_m - R_{mc})/R_{mc}$. The points are averaged over 112 simulations or a total of approximately 8×10^6 samples of $b(t)$.

$$D^{-1} \ll \Delta \ll D/h^2. \tag{19}$$

Note that the scaling ranges (17) and (19) increase as the transition is approached since $h \sim (R_m - R_{mc})$ (see Fig. 3).

(4) *Probability distribution of $b(t)$.* Picking a time t randomly from the range of times over a long time series of $b(t)$, the value of $b(t)$ at that instant is a random variable. We denote the probability distribution function of b by $\hat{P}(b)$. Operationally, $\hat{P}(b)$ can be estimated by choosing many random times and histogramming. It is predicted that $\hat{P}(b)$ has a power law behavior in b

$$\hat{P}(b) \sim b^\gamma, \quad \gamma = (h/D) - 1, \tag{20}$$

for $b \ll b_{max}$.

To summarize, Eq. (14) characterizes the scaling of the bursting behavior with R_m. Equations (15)–(20), in contrast, address the characteristics of the $b(t)$ time series at a *fixed* small value of $(R_m - R_{mc})/R_{mc} > 0$. Equations (15)–(19) characterize the bursts,[30] while Eq. (20) characterizes the small magnetic fluctuations between bursts.

C. Results for $R_m > R_{mc}$, above transition

The simulation results verifying the presence of the scalings given in Eqs. (14)–(20) are shown, respectively, in Figs. 7–10.

Figure 7 shows the results of 112 simulations of the LOM. The plot shows the linear behavior of the average value of $b(t)$ vs $(R_m - R_{mc})/R_m$ (where $R_{mc} = 2.193$ for the LOM) as predicted by Eq. (14). The LOM was used because the time to compute similar data for the $K = 6$ model (HOM) was prohibitively long due to the necessity of doing long runs for many values of R_m. This is in contrast to verifying the scalings (15), (18), and (20) which require only a single long run at one fixed value of R_m, and for which we have been able to use our HOM. We note that the LOM and the HOM give the same results for the scalings (15), (18), and (20), and we take this as evidence that the scaling (14), verified in Fig. 7 with the LOM, should apply to the HOM as well.
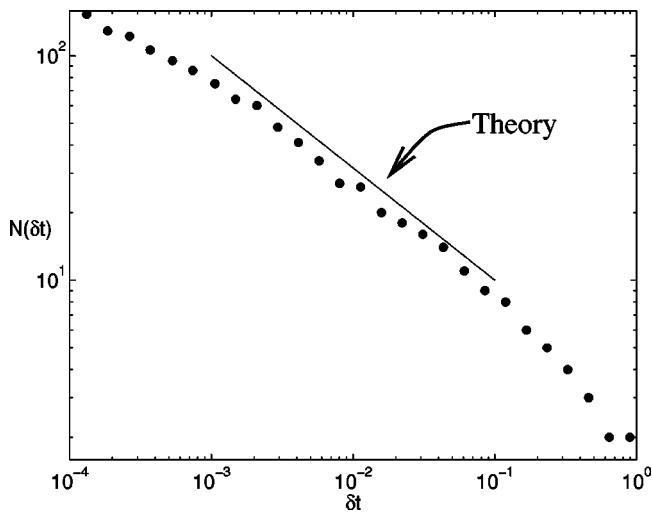
FIG. 8. Fractal dimension of the set of burst times above transition. The predicted scaling is $N(\delta t) \sim (\delta t)^{-1/2}$, Eq. (15), for the range $10^{-3} \ll \delta t \ll 10^{-1}$. The points marked ● were computed by measuring burst times from four simulations with a total aggregate running time of approximately 6×10^4 time units (δt is normalized by the total running time) using a threshold of $b_0 = 0.79$, at parameter $R_m = 7.96$.

Figure 8 shows $N(\delta t)$ vs δt, for the HOM with $R_m = 7.96 > R_{mc} = 7.88$, plotted on a log-log scale. According to (15)–(17) this plot should be linear with slope $-d = -\frac{1}{2}$ (solid line in Fig. 8) in the range $10^{-3} \ll \delta t \ll 10^{-1}$ [Eq. (17)], where δt is normalized to the total running time. The data in this range appear to conform well to the scaling Eq. (16).

In Fig. 9 we plot the probability distribution function of interburst times versus the interburst time to show that the scaling Eq. (18) holds for the converged, HOM, system. The solid line in the figure has the theoretical slope of $-\frac{3}{2}$, and the extent of this line indicates the expected scaling range given in Eq. (19). Our result is robust to the choice of thresh-
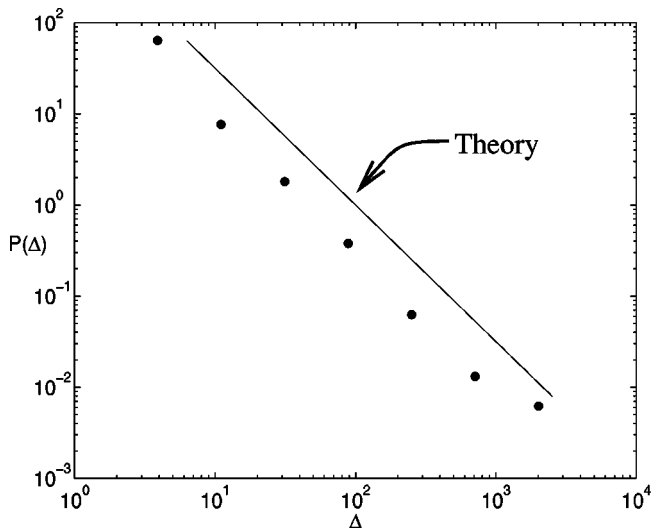

FIG. 9. Distribution of interburst times slightly above transition ($R_m = 7.96 > R_{mc}$). The predicted scaling is $P(\Delta) \sim \Delta^{-3/2}$, Eq. (18). The points marked ● were computed by measuring burst times from the traces with a total running time of approximately 7000 time units using a threshold of $b_0 = 0.8$ [see Fig. 1(b)]. The offset line has the predicted slope $-\frac{3}{2}$.
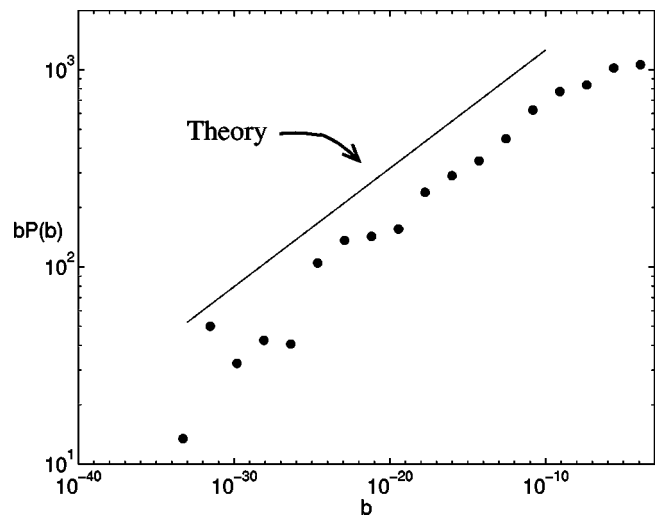

FIG. 10. Probability distribution of $b(t)$, $\hat{P}(b)$ after transition ($R_m > R_{mc}$). The slope of the offset line is $h/D = 0.13$, indicating a signature scaling of $\hat{P}(b) \sim b^{h/D-1}$. Data were taken at $R_m = 7.96$; see caption to Fig. 4 for details.

old (in this case, $b_0 = 0.8$); varying the threshold value between $b_0 = 0.6$ and $b_0 = 1.1$ did not change the scaling.

Figure 10 shows a log-log plot of $b\hat{P}(b)$ vs b obtained by applying the histogram procedure with an ensemble of b values generated by sampling $b(t)$ at many evenly spaced times t over the duration of three long time series. The data were taken at $R_m = 7.96 (R_m > R_{mc})$. Also plotted in Fig. 10 is a line of slope $h/D = 0.13$, which is the slope predicted by Eq. (20). The data conform reasonably well to this prediction.

D. Below threshold ($R_m < R_{mc}$) with a small applied stimulus

Just before transition ($R_m < R_{mc}$) the function $b(t)$ bursts when a small, uniform, external magnetic field, $\mathbf{B} = B_0 \hat{z}$, is applied (see Fig. 2). Equation (15) is also predicted to hold[22] in this case but in the range

$$D^{-1} \ll \delta t \ll \frac{(\ln(D/B_0^2))}{D}.$$

Figure 11 confirms this prediction using the HOM. The scaling range for δt in this case is $10^{-2} \ll \delta t \ll 10^{-1}$.

Figure 12 shows our numerical estimate (using the HOM) of $b\hat{P}(b)$ vs b for $R_m = 7.76 (R_m < R_{mc} = 7.88)$. These data were taken with an applied external field with magnitude $B_0 = 0.166$. The offset line is the theoretically predicted slope of $h/D = -0.17$. (Note that in contrast to the case $R > R_{mc}$, Fig. 10, the predicted slope is negative because now $h < 0$.) The scaling is predicted to hold for $b_{max} \gg b \gg B_0$, where $b_{max} \approx 2.6$. The data are seen to be roughly consistent with Eq. (20).

E. Possibility of hysteretic dynamo onset

Finally we note that in Ref. 17 it is emphasized that blowout bifurcations can be either nonhysteretic (supercritical) or hysteretic (subcritical). In our article, since our MHD
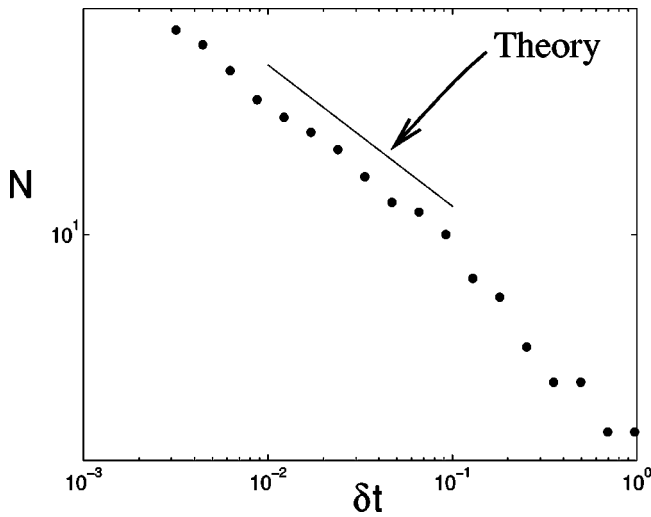
FIG. 11. Fractal dimension of the set of burst times, below transition ($R_m = 7.76 < R_{mc}$) with an externally applied magnetic field. The predicted scaling is $N(\delta t) \sim (\delta t)^{-1/2}$, Eq. (15), for the range $10^{-2} \ll \delta t \ll 10^{-1}$. The offset line has slope $-\frac{1}{2}$. The external field had a magnitude of $B_0 = 0.166$.

simulation gives a nonhysteretic blowout bifurcation, we have only discussed this case. We point out, however, that, for a different situation (e.g., different forcing, geometry, or boundary conditions), it may be possible that the bifurcation to dynamo action will be hysteretic. In such a case, a previously developed[29] phenomenology and scalings for hysteretic blowout bifurcations would be expected to apply.

V. CONCLUSION

We have shown that the onset of MHD dynamo action can have an intermittently bursting character and that this results from a blowout bifurcation at the transition to dy-
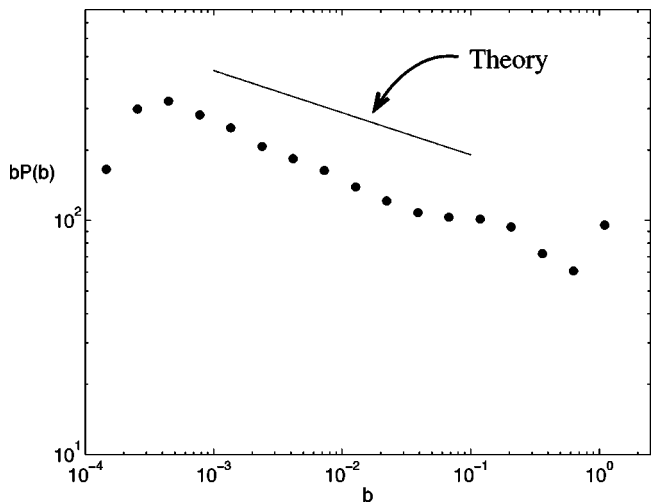

FIG. 12. Probability distribution of b, $\hat{P}(b)$, below transition ($R_m < R_{mc} \cong 7.88$) with a small externally applied field. The slope of the offset line is $h/D = -0.17$, where $h = -0.0044$ and $D = 0.026$. Data were taken at $R_m = 7.76$. The external field had magnitude $B_0 = 0.166$. The predicted scaling range is $b_{max} \gg b \gg B_0$, where $b_{max} \approx 2.6$ is the largest value attained by b in this time series.

namo action. In particular, we have verified the presence of this transition by computing the scaling behavior of various measured model quantities.

Although the boundary conditions used in our simulation are not appropriate for constructing an accurate, detailed, model of any of the dynamo experiments being carried out in laboratories, we believe that our result applies to such systems. The blowout bifucation is conjectured to be typical[17] of dynamical systems possessing the attributes (i)–(iv) presented in Sec. II. The MHD dynamo equations and at least one experimental system[14] possess these attributes, and we have verified numerically that our simulation of the MHD equations undergoes the blowout bifurcation. Based on this evidence we predict that experimental MHD dynamo systems with unconstrained turbulent flow should experience a blowout bifurcation as their transition to dynamo action and that, if this transition is nonhysteretic, it will be characterized by intermittently bursting magnetic fields.

We suggest three specific experimental tests of this prediction. First, just below the transition, pulse-decay measurements could verify the existence of a broad finite time Lyapunov exponent distribution comparable to Fig. 4. Second, applying a small seed field (which is, in fact, usually unavoidable in an experimental setting) would cause bursts similar to Fig. 2 with a fractal set of bursts times (Fig. 11). Finally, an experiment performed above transition should also show a fractal set of burst times (similar to Fig. 8).

ACKNOWLEDGMENTS

[1]H. K. Moffatt, *Magnetic Field Generation in Electrically Conducting Fluids* (Cambridge University Press, Cambridge, 1978); F. Krause and K.-H. Rädler, *Mean-Field Magnetohydrodynamics and Dynamo Theory* (Pergamon, Oxford, 1980); E. N. Parker, *Cosmical Magnetic Fields* (Clarendon, Oxford, 1979).

[2]E. Bullard and H. Gellman, Philos. Trans. R. Soc. London **A247**, 27 (1954); G. Glatzmaier and P. H. Roberts, Phys. Earth Planet. Inter. **91**, 63 (1995); R. Kleva and J. F. Drake, Phys. Plasmas **2**, 4455 (1995).

[3]M. L. Dudley and R. W. James, Proc. R. Soc. London, Ser. A **25**, 404 (1989).

[4]D. Galloway and U. Frisch, J. Fluid Mech. **180**, 557 (1987); Geophys. Astrophys. Fluid Dyn. **36**, 53 (1987).

[5]S. Rüdiger, F. Feudel, and N. Seehafer, Phys. Rev. E **57**, 5533 (1998).

[6]S. Childress and A. D. Gilbert, *Stretch, Twist, Fold: The Fast Dynamo* (Springer-Verlag, New York, 1995).

[7]E. Ott, Phys. Plasmas **5**, 1636 (1998); J. M. Finn and E. Ott, Phys. Fluids **31**, 2992 (1988); C. Reyl, E. Ott, and T. M. Antonsen, Phys. Plasmas **3**, 2564 (1996).

[8]B. J. Bayly and S. Childress, Geophys. Astrophys. Fluid Dyn. **44**, 211 (1988).

[9]A. K. Galitis, B. G. Karasev, I. R. Kirillov, O. A. Lielausis, S. M. Luzhanskii, and A. P. Ogorodnikov, Magnetohydrodynamics **23**, 349 (1987); A. Gailitis, O. Lielausis, E. Dement'ev, E. Platacis, and A. Cifersons, Phys. Rev. Lett. **84**, 4365 (2000).

[10]U. Müller and R. Stieglitz, Naturwissenschaften **87**, 381 (2000). The bursting phenomena we predict is not seen in the Karlsruhe experiment because, in their device the liquid sodium is constrained to flow in a parallel square array of 54 specially configured tubes. This means that the fluctuation scales of the flow ($\sim$ pipe diameter) are much smaller than that

of the active magnetic field ($\sim$ the size of the whole array). Thus the flow generating the magnetic field is effectively nonturbulent; only the velocity cross sectionally averaged over a pipe is important and, due to the pumping system, is nearly steady. This situation is very different from what is planned for the other experiments[11–14] where the flow is unconstrained and large-scale turbulent fluctuations, on the scale of the device size, will be present. (Note also that these other experiments much more closely model the unconstrained situations occurring in nature.)

[11] P. Odier, J.-F. Pinton, and S. Fauve, Phys. Rev. E **58**, 7397 (1998).

[12] C. Forrest, private communication (1999).

[13] S. Colgate, private communication (1999).

[14] N. Peffley, A. Cawthorne, and D. Lathrop, Phys. Rev. E **61**, 5287 (2000).

[15] L. Yu, E. Ott, and Q. Chen, Phys. Rev. Lett. **65**, 2935 (1990); L. Yu, E. Ott, and Q. Chen, Physica D **53**, 102 (1991).

[16] H. Fujisaka *et al.*, Prog. Theor. Phys. **76**, 1198 (1986).

[17] E. Ott and J. C. Sommerer, Phys. Lett. A **188**, 39 (1994).

[18] H. Fujisaka and T. Yamada, Prog. Theor. Phys. **74**, 919 (1985); **75**, 1087 (1986).

[19] N. Platt, S. M. Hammel, and J. F. Heagy, Phys. Rev. Lett. **70**, 3498 (1994).

[20] J. F. Heagy, N. Platt, and S. M. Hammel, Phys. Rev. E **49**, 1140 (1994).

[21] S. C. Venkataramani, T. M. Antonsen, Jr., E. Ott, and J. C. Sommerer, Phys. Lett. A **207**, 173 (1995).

[22] S. C. Venkataramani, T. M. Antonsen, Jr., E. Ott, and J. C. Sommerer, Physica D **96**, 66 (1996).

[23] E. Covas, P. Ashwin, and R. Tavakol, Phys. Rev. E **56**, 6451 (1997). This paper deals with a dynamo blowout bifurcation, but the bifurcation is very different from the one we consider here; in particular, it does not represent the onset of dynamo action.

[24] P. Ashwin, J. Buescu, and I. Stewart, Phys. Lett. A **193**, 126 (1994).

[25] S. A. Orszag, Stud. Appl. Math. **50**, 293 (1971).

[26] S. A. Orszag, Stud. Appl. Math. **51**, 253 (1972).

[27] C. Canuto, M. Y. Hussaini, A. Quateroni, and T. A. Zang, *Spectral Methods in Fluid Dynamics*, Springer Series Comput. Phys. (Springer, Berlin, Heidelberg, 1987).

[28] B. Galanti, P. L. Sulem, and A. Pouquet, Geophys. Astrophys. Fluid Dyn. **66**, 183 (1992).

[29] E. Ott, J. C. Alexander, I. Kan, J. C. Sommerer, and J. A. Yorke, Physica D **76**, 384 (1994).

[30] Another characterization of the bursts is the frequency power spectrum, $S(\omega)$, of the $b(t)$ time series, which is predicted[16,18,21] to have a power law range $S(\omega) \sim \omega^{-1/2}$. However, the scaling $S(\omega) \sim \omega^{-1/2}$ has proven difficult to detect in previous low-dimensional chaos studies[21] where very long runs were required. Here we have found similar behavior using our $K=1$ model (LOM), obtaining $S(\omega) \sim \omega^{-1/2}$ for sufficiently long runs. At any rate, due to this difficulty, we suggest that the fractality of the burst times and the pdf of interburst intervals [Eqs. (15)–(19)] may be more useful ways of characterizing bursting.